Magnetoelastic coupling in the triangular lattice antiferromagnet $CuCrS_2$

Julia C. E. Rasch,[1,2,*] Martin Boehm,[1] Clemens Ritter,[1] Hannu Mutka,[1] Jürg Schefer,[2] Lukas Keller,[2] Galina M. Abramova,[3] Antonio Cervellino,[4] and Jörg F. Löffler[5]

[1]*Institut Laue-Langevin, 6 Rue Jules Horowitz, BP 156, 38042 Grenoble Cedex 9, France*

[2]*Laboratory for Neutron Scattering, ETH Zurich and Paul Scherrer Institut, CH-5232 Villigen PSI, Switzerland*

[3]*L.V. Kirensky Institute of Physics, SB RAS, Krasnoyarsk 660036, Russia*

[4]*Swiss Light Source, Paul Scherrer Institut, CH-5232 Villigen PSI, Switzerland*

[5]*Laboratory of Metal Physics and Technology, Department of Materials, ETH Zurich, 8093 Zurich, Switzerland*

(Received 28 July 2009; revised manuscript received 24 August 2009; published 24 September 2009)

$CuCrS_2$ is a triangular lattice Heisenberg antiferromagnet with a rhombohedral crystal structure. We report on neutron and synchrotron powder diffraction results which reveal a monoclinic lattice distortion at the magnetic transition and verify a magnetoelastic coupling. $CuCrS_2$ is therefore an interesting material to study the influence of magnetism on the relief of geometrical frustration.

DOI: 10.1103/PhysRevB.80.104431 PACS number(s): 75.25.+z, 61.05.−a, 75.80.+q, 64.70.Nd

I. INTRODUCTION

Heisenberg antiferromagnets on a triangular lattice are subject to ongoing interest due to a strong correlation between lattice geometry and electronic and magnetic properties. Geometrical frustration plays a key role in compounds with triangular arrangement of magnetic moments[1] and leads to particular characteristics including incommensurate spin structures and multiferroic properties.[2] Ternary triangular lattice dioxides and dichalcogenides have in common to crystallize in a layered structure with strong crystalline anisotropy perpendicular to the layers (mainly space group $R3m$ and $R\bar{3}m$). In chromium based dioxides the most commonly established magnetic structure is a quasi-two-dimensional 120° spin structure, typical for Heisenberg exchange on a triangular lattice, with a weak interlayer coupling e.g., in $AgCrO_2$,[3] $PdCrO_2$,[4] $NaCrO_2$,[5] and $CuCrO_2$.[6] The latter two also show a magnetoelectric coupling where the spin structure induces ferroelectricity.[7,8] Ternary chromium dichalcogenides have been less intensively studied, and show a variety of different magnetic structures ranging from a 120° spin structure in $LiCrS_2$ (Ref. 9) over a commensurate magnetic structure in $KCrS_2$ (Ref. 10) to a helix with an in-plane spin orientation in $NaCrS_2$.[10]

The compound under investigation, $CuCrS_2$, has drawn attention as an ionic conductor[10] and is assumed to exhibit a spin glass state under the substitution of chromium ions by vanadium.[11,12] A microscopic temperature-dependent investigation of magnetic and crystallographic properties is, however, lacking. $CuCrS_2$ crystallizes in space group $R3m$ at room temperature.[13] The basic atomic structure consists of covalent-ionic bound S-Cr-S layers separated by a van der Waals gap causing strong crystalline anisotropy perpendicular to the layers. Isolated CrS_2 is metastable and occurs only with an electron donor, therefore monovalent Cu^+ cations are intercalated between (CrS_2) sandwiches.[10,14] The magnetic Cr^{3+} ions with spin $S=3/2$ form triangular layers which are shifted by $(\frac{1}{3},\frac{2}{3},\frac{2}{3})$ and $(\frac{2}{3},\frac{1}{3},\frac{1}{3})$, as shown in the inset of Fig. 1. The nearest-neighbor intralayer Cr-Cr distance of 3.48 Å is small compared to the interlayer Cr-Cr distance of 6.55 Å. The magnetic exchange within the layers over Cr-S-Cr pathways is expected to be much stronger than the interlayer exchange via Cr-S-Cu-S-Cr bonds. Hence, one would expect to find the crystalline anisotropy to be reflected in the magnetic system, as described in the dioxides. Nevertheless, early neutron powder diffraction experiments on $CuCrS_2$ revealed a three-dimensional magnetic ordering below $T_N=40$ K into a complex helical structure with an incommensurate magnetic propagation vector.[15] This phenomenon cannot be explained without interlayer exchange interactions which must be of the same order of magnitude as the intralayer exchange. An estimation of exchange constants is given in the discussion. The particularity of $CuCrS_2$ is a strong lattice effect exactly at T_N. We assume that the lattice distortion provides a channel for the system to escape the two-dimensional (2D) triangular arrangement, usually leading to magnetic frustration. The consequences on the lattice and magnetic structure throughout the phase transition are sub-

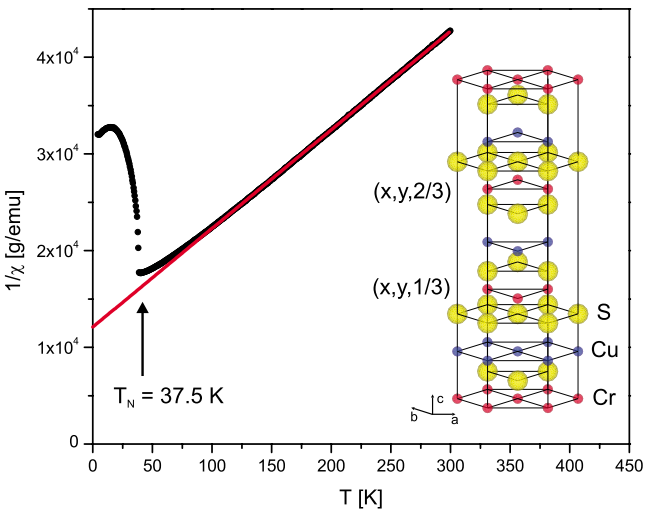

FIG. 1. (Color online) Inverse magnetic susceptibility of $CuCrS_2$ measured at $H=10$ kOe as a function of temperature. An antiferromagnetic anomaly at $T_N=37.5$ K is clearly visible. The red solid line shows the Curie-Weiss fit to the paramagnetic part of the curve. Inset: structural unit cell of $CuCrS_2$ at room temperature with space group $R3m$.

ject of this paper. A similar lattice effect occurs in triangular lattice $CuFeO_2$, where a crystal symmetry lowering is found to lift the degeneracy of the frustrated spin system[16] together with multiferroic properties induced by a magnetic field or non-magnetic impurities.[17,18] Strong spin-lattice effects are also found in three-dimensional (3D) frustrated systems, as shown for the well-known pyrochlore spinel $ZnCr_2O_4$.[19] The compound was found to undergo a Spin-Peierls-like phase transition which comprises an energy lowering through a lattice distortion and the opening of an energy gap. The origin of this gap has been explained by clustering of the Cr moments into weakly interacting antiferromagnetic loops.[20] Although the formation of spin cluster has been clarified, the magnetic structure is not fully understood.[21] We claim to see a similar effect on a triangular lattice and report in this paper on the detailed magnetic structure.

II. EXPERIMENTAL DETAILS

The polycrystalline sample of $CuCrS_2$ was synthesized by solid state reaction of the pure elements. A detailed description is given elsewhere.[22] Single crystals were grown by chemical vapor transport in an evacuated quartz ampoule with $p \leq 10^{-4}$ mbar. A temperature gradient was applied over 30 cm ampoule length between 900 and 950 °C during three weeks. The furnace was then cooled at a cooling rate of 1 K/min to room temperature. The resulting single crystals are thin platelets which possess a black shiny surface with the [001] direction perpendicular to it. The size of the surface ranges from 10 to 100 mm^2 with a typical thickness of 0.2 mm. The stoichiometry of the samples was checked by energy dispersive x-ray spectroscopy and verified in case of the polycrystalline powder. The single crystals contain an impurity phase of not more than 10% $CuCr_2S_4$. Systematic variations of growth conditions in order to avoid the impurity phase, produced crystals too thin (<10 μm) and unstable for use in neutron scattering experiments.

Neutron powder diffraction measurements were carried out on the cold diffractometer DMC at the neutron spallation source SINQ, Paul Scherrer Institut (PSI) and the thermal diffractometer D1A at the Institut Laue-Langevin (ILL) with $\lambda = 2.46$ Å and $\lambda = 1.91$ Å, respectively, in a standard orange cryostat. Single crystal diffraction experiments were performed on the thermal instrument TriCS (Ref. 23) (SINQ) with $\lambda = 1.18$ Å in a four-circle Eulerian cradle and on the three-axis spectrometer IN3 (ILL) with $\lambda = 2.36$ Å. High-resolution synchrotron radiation powder diffraction patterns

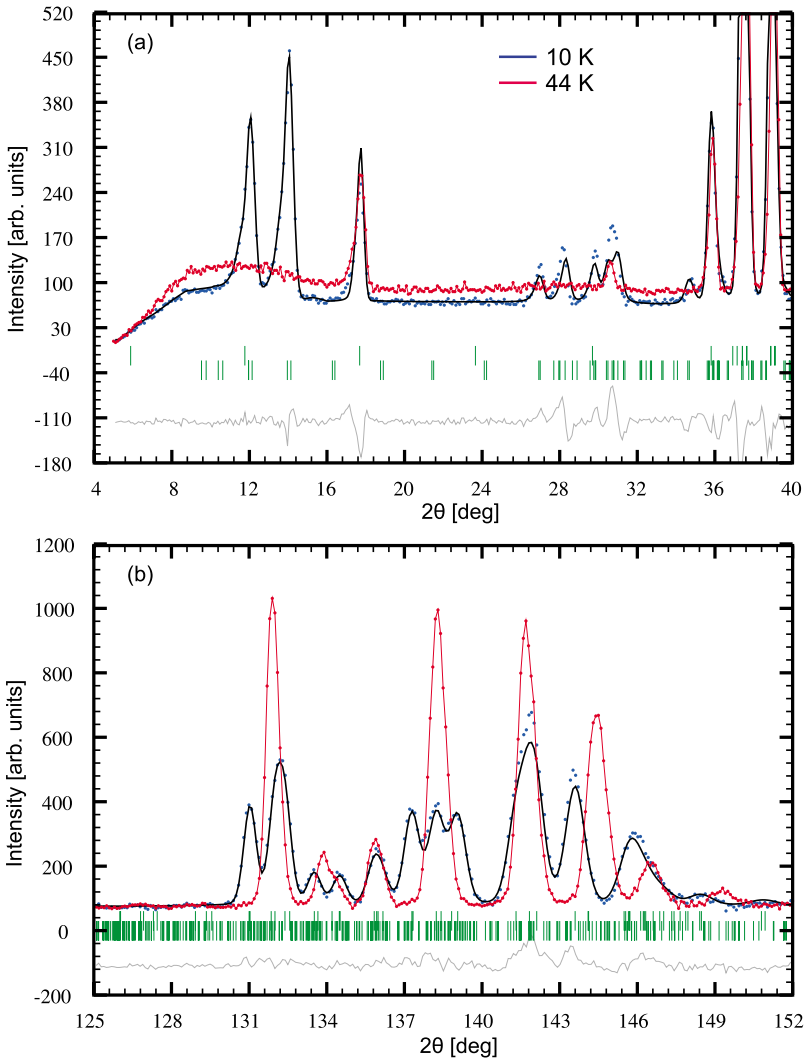

FIG. 2. (Color online) Neutron powder diffraction data taken on D1A at 10 K (refined) and 44 K (raw data). The refinement of the 10 K data with a nuclear and magnetic phase is indicated by a black solid line. The difference between refinement and observed data at 10 K is shown in gray. (a) depicts the low 2θ region where magnetic reflections are visible which disappear at 44 K and (b) shows the high 2θ region where a splitting of the nuclear Bragg peaks below the transition is observable.

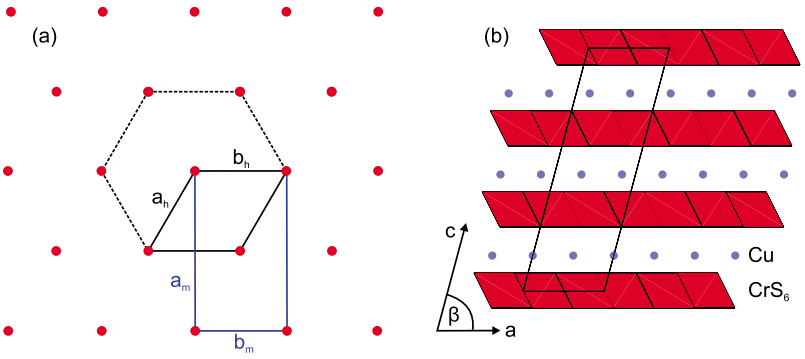

FIG. 3. (Color online) (a) Correlation of the rhombohedral unit cell in hexagonal description ($R3m$) and the monoclinic unit cell (Cm). (b) Influence of the monoclinic angle β on the layers. The angle is overdrawn to show the effect of distortion; actually β only deviates slightly from 90°.

were collected at the powder diffraction station of the Swiss Light Source Materials Science (SLS-MS) beamline at an incident photon energy of $\lambda=0.621\ 288(1)$ Å. The sample was mounted in a Janis cryostat in 0.2 mm Lindemann capillaries which spun at approximately 10 Hz during the 2θ scan to avoid preferred orientation. The collected neutron and x-ray diffraction data were refined using the program Fullprof[24] based on Rietveld refinement.

Magnetic susceptibility measurements were carried out on a physical properties measurement system over a temperature range of 4–300 K with an external field of 10 kOe and on a superconducting quantum interference device (SQUID) magnetometer for temperatures up to 400 K.

III. RESULTS

Figure 1 shows the temperature dependence of the inverse magnetic susceptibility of the powder sample with an antiferromagnetic transition at $T_N=37.5$ K. From the linear part of the curve the paramagnetic Curie-Weiss temperature could be determined to $\Theta_{CW}=-118.5(1)$ K and the effective magnetic moment amounts to $\mu_{exp}=3.75(1)\mu_B$ close to the spin-only value $\mu_{S_{3/2}}=3.87\mu_B$. The magnetization curve of the single crystal, measured up to 400 K (not shown), indicates a superposition of the antiferromagnetic transition of $CuCrS_2$ at $T_N=37.5$ K and a ferromagnetic transition of $CuCr_2S_4$ at $T_c=377$ K.[25]

A good measure for the degree of frustration is the ratio $|\Theta_{CW}|/T_N$ which is in case of $CuCrS_2$ only 3.16 and therefore rather small to infer a strongly frustrated system with values usually larger than 10.[26]

Neutron powder diffraction data taken on D1A and DMC at different temperatures show strong magnetic Bragg peaks emerging below the magnetic transition, i.e., $T_N=37.5$ K. This observation must be related to a magnetic ordering of the system. At higher diffraction angles 2θ, accessible on D1A, a splitting of nuclear Bragg peaks is also observable, which indicates a symmetry lowering of the crystal structure. The pattern taken above and below the transition at 44 and 10 K, respectively, are shown in Fig. 2. The pictures (a) and (b) show the refinement of the low temperature data at 10 K with two phases, nuclear and magnetic, superimposed by the raw data pattern at 44 K. Above T_N the Cr^{3+} moments show no long range order anymore, but localized Cr^{3+} moments still cause paramagnetic scattering. Therefore, the difference in background intensity between spectra taken at 10 and 44 K at low angles 2θ [Fig. 2(a)] can be explained by an angle dependence of the paramagnetic scattering due to the magnetic form factor. The effect is negligible at higher angles 2θ [Fig. 2(b)].

The structural transition indicated by a splitting of the nuclear Bragg peaks in the low temperature phase could be identified as a symmetry lowering from rhombohedral space group $R3m$ (160) to monoclinic space group Cm (8). The relation between both unit cells is given in Fig. 3, as well as a visualization of the monoclinic angle β. The introduction of a monoclinic angle β causes a slight shear movement of the layers in the ab plane. Lattice parameters and crystal symmetry at 300 K and 10 K taken at the SLS-MS beamline are listed in Table I. Refinements with space group Cm describe the splitting of the Bragg peaks in the nuclear phase very well [see Fig. 2(b)]. Above the phase transition all three lattice parameters, depicted in Figs. 4(a)–4(c), decrease with cooling. Upon further cooling a and c show a discontinuous jump toward lower values, whereas b increases quickly. The complementarity of the in-plane lattice constants a and b will later be explained by a distortion of the Cr hexagon.

The refinement of magnetic intensities was done with a magnetic propagation vector documented earlier[15] which was redefined on the monoclinic lattice and fits well to the magnetic Bragg peaks [see Fig. 2(a)]. The propagation vector

TABLE I. Lattice parameters of $CuCrS_2$, refined with space group $R3m$ at 300 K and Cm at 10 K. Data were collected at the SLS-MS beamline with wavelength $\lambda=0.621\ 288(1)$ Å.

Temperature	300 K	10 K
Space group	$R3m$	Cm
Nr.	160	8
	rhombohedral	monoclinic
a [Å]	3.484543(4)	5.99923(1)
b [Å]	3.484543(4)	3.491502(5)
c [Å]	18.71878(2)	18.64794(3)
α [°]	90	90
β [°]	90	89.93727(8)
γ [°]	120	90
R_{Bragg}[%]	4.13	3.83

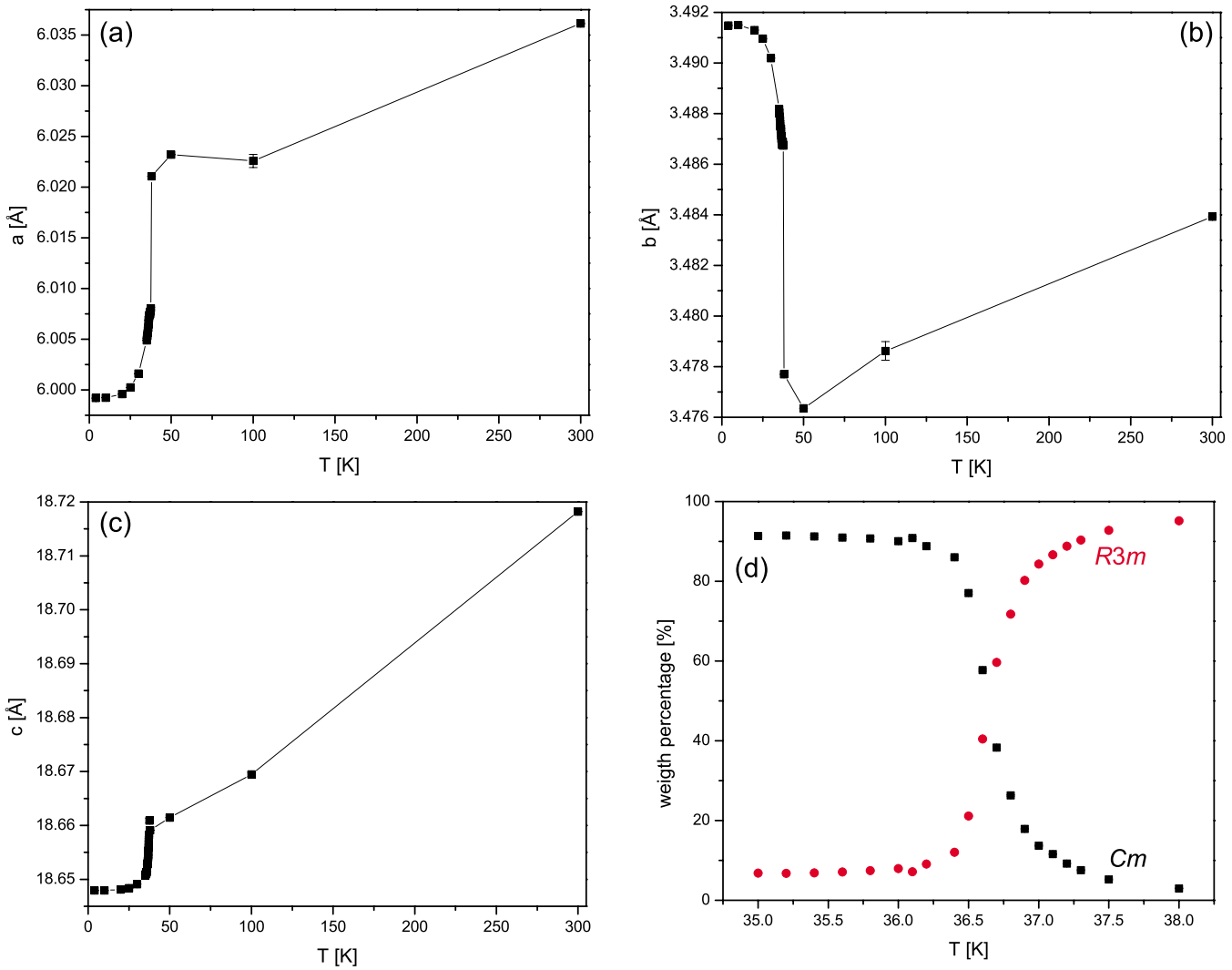

FIG. 4. (Color online) Temperature evolution of the lattice parameters a, b, and c corresponding to (a) to (c), extracted from synchrotron data, in monoclinic description *Cm*. For better comparability the refinements for $T>37$ K were performed in the monoclinic description with $\beta=90°$ and $a=\sqrt{3}b$. (d) shows the refined weight percentage of both the high temperature *R*3*m* phase (circles) and the low temperature *Cm* phase (squares) through the transition. The error bars are smaller than the symbols.

$\boldsymbol{k}=(-0.493,-0.087,1.25)$ in relative length units (r.l.u.), describes a three-dimensional helical arrangement of magnetic moments originating from Cr^{3+} ions. The best fitting results were obtained with no magnetic moment on the Cu atoms, from which we conclude that Cu is in oxidation state Cu^{+}, corresponding to the stoichiometry of the sample. Neutron single crystal diffraction experiments were performed on IN3 (ILL) and TriCS (SINQ) to confirm the rather unusual magnetic propagation vector and to avoid artifacts from the powder refinement. Magnetic Bragg peaks were found at several positions in 3D reciprocal space, corresponding to the propagation vector obtained from powder measurements and verified the incommensurate magnetic structure. The intensity of all magnetic peaks, including the strongest (003)-$\boldsymbol{k}$, vanishes at $T_N=37.5$ K but shows different temperature behavior than in the powder, i.e., a varying critical exponent extracted from $M_s\sim\sqrt{I}$ close to the phase transition. The values are 0.08(4) for the powder compared to 0.5(1) for the single crystal. This is possibly due to an internal magnetic field in the single crystal caused by the ferromagnetic impurity $CuCr_2S_4$ which slows down the transition. The magnetic intensity is saturated for $T<30$ K. Since T_N and $\boldsymbol{k}$ coincide for powder and single crystal in both susceptibility and diffraction data, we conclude that the presence of $CuCr_2S_4$ does not disturb the measurement of the magnetic structure in $CuCrS_2$ at low temperatures.

A detailed analysis of the D1A powder data revealed an interesting coupling between magnetic ordering and structural distortion. The temperature dependencies of the magnetic intensity in the strongest Bragg peak at $2\theta=13.96°$ and the monoclinic angle β show reverse behavior, depicted in Fig. 5. As the sample is cooled below T_N the magnetic ordering sets in and a deformation of the lattice develops simultaneously, expressed by a monoclinic angle β deviating from 90°. Although the deviation of β from a higher symmetric value seems to be tiny it is crucial to solve the low temperature crystal structure. Figure 5 shows the mutual influence of lattice distortion and magnetic ordering.

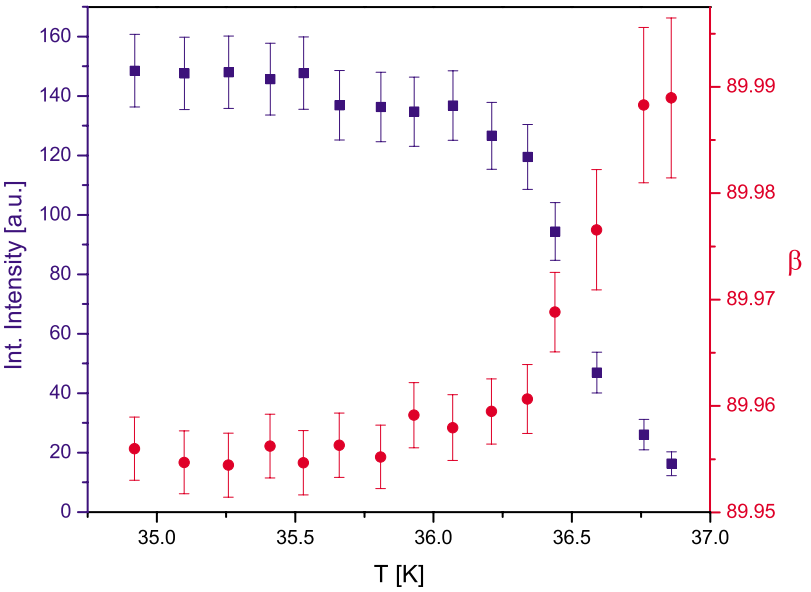

FIG. 5. (Color online) Intensity of the strongest magnetic Bragg peak at $2\theta=13.96°$ (squares) and the monoclinic angle β (circles) as a function of temperature, extracted from neutron powder diffraction data taken on D1A. While cooling the sample, the ordering of magnetic moments and the lattice distortion set in simultaneously.

Additional to the interlayer shear movement, another type of intralayer structural distortion was identified from synchrotron powder measurements at the SLS-MS beamline. At high temperatures the in-plane chromium lattice describes a symmetric hexagon. Upon cooling the symmetric chromium environment distorts, such that four of the six equal Cr-Cr bonds contract and two elongate. This causes a flattening of the hexagon, as schematically shown in the inset of Fig. 6, and leads to nearest-neighbor (d_1) and next nearest-neighbor (d_2) Cr bonds. The Cr-Cr distances d_1 and d_2 show the same temperature evolution as the interlayer distortion (see Fig. 6). In addition, d_2 coincides with the lattice parameter b, which explains its unconventional temperature dependence below T_N.

These two types of distortions, the interlayer shear movement by an angle β and the intralayer hexagonal symmetry breaking, seem to play an important role for the magnetic ordering. The system is able to select a magnetic ground state due to the relief of geometrical frustration.

IV. DISCUSSION

The analysis of the diffraction pattern at different temperatures shows an abrupt change of Cr-Cu (lattice parameter c) and Cr-Cr distances (d_2) below the phase transition. Usually a contraction causes strain in the lattice which is proportional to the square of the atomic displacement u and increases elastic energy $\sim u^2$. A phase transition has to be energetically favorable, which means that the gain in elastic energy must be compensated. Using the example of the phase transition in solid oxygen, Rastelli *et al.*[27] state that a first-order transition is feasible when the ground-state energy of the rhombohedral phase equals the ground-state energy of the monoclinic phase. Synchrotron powder diffraction data confirm a first-order transition in $CuCrS_2$ identified from a residual rhombohedral $R3m$ phase even at the lowest temperature, depicted in Fig. 4(d). Mixed-phase regimes are characteristic for first-order phase transitions.[28] This may explain the deviation of the critical exponent 0.08(4) from

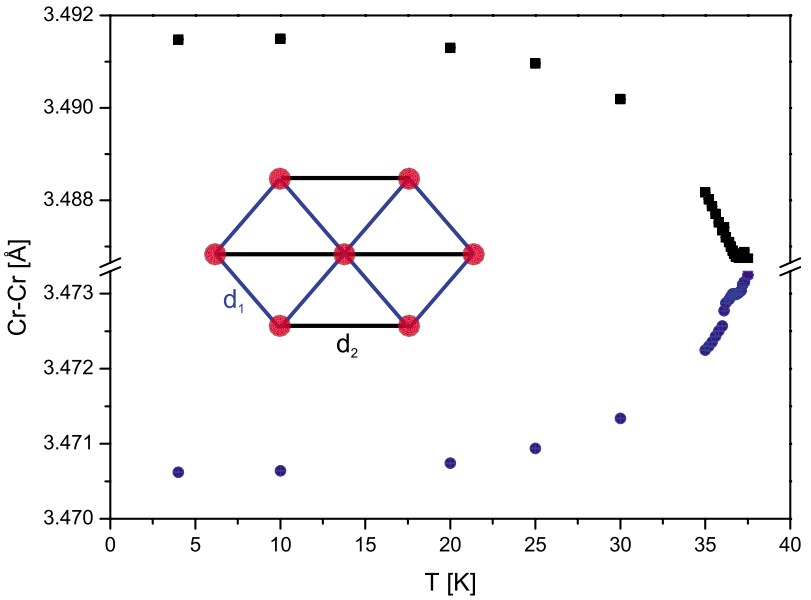

FIG. 6. (Color online) Temperature dependence of in-plane Cr-Cr bonds d_1 (circles) and d_2 (squares) measured by synchrotron powder diffraction. Inset: different kinds of chromium bonds and their influence on the distortion. The deformation is overdrawn for better illustration.

common models (Ising, XY or Heisenberg), since it is merely defined for second-order phase transitions. A reduction of the total free energy can only be achieved by a decrease in magnetic energy. For discussion we assume three different magnetic exchange paths in $CuCrS_2$ comprising in-plane nearest-neighbors J_1 (along d_1, see Fig. 6) and next nearest-neighbors J_2 (along d_2) and interplane exchange J_3.

The intralayer exchange integrals J_1 and J_2 can have two origins, a direct antiferromagnetic interaction of neighboring Cr^{3+} ions or an indirect superexchange interaction via S^{2-} which would be ferromagnetic due to the Cr-S-Cr angle of 90°. The susceptibility curve shows antiferromagnetic behavior, and we can therefore neglect the ferromagnetic superexchange path. Interlayer exchange is presumably mediated by Cu^+ ions through the path Cr-S-Cu-S-Cr. It needs to be taken into account to explain the three-dimensional magnetic structure. The contraction of Cr-Cu bonds through the transition seems to provide evidence for the important role of the interlayer Cr-Cu-Cr exchange path. The ratio between the in-plane and interplane exchange constants can be calculated for a rhombohedral antiferromagnet with a helical propagation vector.[27] For $CuCrS_2$ we find a surprisingly high ratio $J_3/J_1=2$, which would imply a very strong interplane coupling. Additional inelastic neutron scattering on powder and single crystals are currently undertaken to verify the validity of this model.

The in-plane distortion of the high temperature symmetric Cr^{3+}-hexagon consists of a deformation where four nearest-neighbors move toward the central Cr^{3+} ion and two nearest-neighbors move away. The transition takes place in order to minimize magnetic energy, as was found in solid oxygen.[29] The two different kinds of intralayer Cr-Cr distances d_1 and d_2 (Fig. 6) may be evidence for the formation of magnetic clusters in $CuCrS_2$, which is supported by preliminary neutron scattering results. It has been found that localized magnetic excitations occur additionally to standard spin waves branches in the spectra. To our knowledge the formation of magnetic clusters in triangular antiferromagnets with spin-lattice coupling has only been theoretically described[30] so far. This phenomenon makes $CuCrS_2$ an interesting candidate for studying new magnetic effects on frustrated lattices.

V. CONCLUSION

From the quasi-two-dimensional layered structure of $CuCrS_2$ one would expect a low dimensional magnetic ordering due to the van der Waals gap between magnetic Cr^{3+} layers. Nevertheless, our measurements show unambiguously that magnetic moments in $CuCrS_2$ order in a fully three-dimensional manner with a helical magnetic propagation vector $\boldsymbol{k}=(-0.493,-0.087,1.25)$. Moreover, the system undergoes a crystallographic transition from rhombohedral $R3m$ to monoclinic Cm at $T_N=37.5$ K, which coincides with susceptibility measurements. Since the ordering of magnetic moments and the lattice distortion occur simultaneously, $CuCrS_2$ has been identified as magnetoelastic material. The system is therefore an interesting candidate for studying spin-lattice effects on a triangular lattice.

ACKNOWLEDGMENTS

We are grateful for support and allocated beam time at the Institut Laue-Langevin (D1A, IN3), Grenoble, France, the spallation neutron source SINQ (TriCS, DMC) and the SLS-MS beamline, both Paul Scherrer Insitut, Villigen, Switzerland. This work was supported by INTAS Grant No. 06-1000013-9002 of the Russian Academy of Science (RAS), Siberian Branch.

*rasch@ill.fr

[1] M. F. Collins and O. A. Petrenko, Can. J. Phys. **75**, 605 (1997).
[2] S.-W. Cheong and M. Mostovoy, Nat. Mater. **6**, 13 (2007).
[3] Y. Oohara, S. Mitsuda, H. Yoshizawa, N. Yaguchi, H. Kuriyama, T. Asano, and M. Mekata, J. Phys. Soc. Jpn. **63**, 847 (1994).
[4] H. Takatsu, H. Yoshizawa, S. Yonezawa, and Y. Maeno, Phys. Rev. B **79**, 104424 (2009).
[5] D. Hsieh, D. Qian, R. F. Berger, R. J. Cava, J. W. Lynn, Q. Huang, and M. Z. Hasan, Physica B **403**, 1341 (2008).
[6] H. Kadowaki, H. Kikuchi, and Y. Ajiro, J. Phys.: Condens. Matter **2**, 4485 (1990).
[7] S. Seki, Y. Onose, and Y. Tokura, Phys. Rev. Lett. **101**, 067204 (2008).
[8] K. Kimura, H. Nakamura, K. Ohgushi, and T. Kimura, Phys. Rev. B **78**, 140401(R) (2008).
[9] A. Lafond, W. Henggeler, H. Mutka, and B. Ouladdiaf, Can. J. Phys. **79**, 1427 (2001).
[10] F. M. R. Engelsman, G. A. Wiegers, F. Jellinek, and B. van Laar, J. Solid State Chem. **6**, 574 (1973).
[11] G. M. Abramova, G. A. Petrakovskii, D. A. Velikanov, A. M. Vorotynov, N. I. Kiselev, R. F. Almukhametov, and V. V. Sokolov, Phys. Met. Metallogr. **100**, S26 (2005).
[12] N. Tsujii and H. Kitazawa, J. Phys.: Condens. Matter **19**, 145245 (2007).
[13] J. A. Wilson and A. D. Yoffe, Adv. Phys. **18**, 193 (1969).
[14] P. F. Bongers, C. F. van Bruggen, J. Koopstra, W. P. F. A. M. Omloo, G. A. Wiegers, and F. Jellinek, J. Phys. Chem. Solids **29**, 977 (1968).
[15] M. Wintenberger and Y. Allain, Solid State Commun. **64**, 1343 (1987).
[16] N. Terada, S. Mitsuda, H. Ohsumi, and K. Tajima, J. Phys. Soc. Jpn. **75**, 023602 (2006).
[17] S. Seki, Y. Yamasaki, Y. Shiomi, S. Iguchi, Y. Onose, and Y. Tokura, Phys. Rev. B **75**, 100403(R) (2007).
[18] T. Kimura, J. C. Lashley, and A. P. Ramirez, Phys. Rev. B **73**, 220401(R) (2006).
[19] S.-H. Lee, C. Broholm, T. H. Kim, W. Ratcliff, and S.-W. Cheong, Phys. Rev. Lett. **84**, 3718 (2000).
[20] S.-H. Lee, C. Broholm, W. Ratcliff, G. Gasparovic, Q. Huang, T. H. Kim, and S.-W. Cheong, Nature (London) **418**, 856 (2002).
[21] V. N. Glazkov, A. M. Farutin, V. Tsurkan, H.-A. Krug von Nidda, and A. Loidl, Phys. Rev. B **79**, 024431 (2009).
[22] R. F. Almukhametov, R. A. Yakshibaev, E. V. Gabitov, A. R. Abdullin, and R. M. Kutusheva, Phys. Status Solidi B **236**, 29

(2003).
[23] J. Schefer, M. Könnecke, A. Murasik, A. Czopnik, Th. Strässle, P. Keller, and N. Schlumpf, Physica B **276-278**, 168 (2000).
[24] J. Rodriguez-Carvajal, Physica B **192**, 55 (1993).
[25] Y. Kamihara, M. Matoba, T. Kyomen, and M. Itoh, Solid State Commun. **132**, 247 (2004).
[26] J. E. Greedan, J. Mater. Chem. **11**, 37 (2001).
[27] E. Rastelli and A. Tassi, J. Phys. C **21**, 1003 (1988).
[28] C. Weißmantel and C. Hamann, *Grundlagen der Festkörperphysik* (Springer-Verlag, Berlin, 1980).
[29] P. W. Stephens and C. F. Majkrzak, Phys. Rev. B **33**, 1 (1986).
[30] C. Jia and J. H. Han, Phys. Rev. B **73**, 172411 (2006).